Geophys. J. R. astr. Soc. (1983) **72**, 691–707

Tidal dynamics in the South China Sea

A. L. Ye* and I. S. Robinson *Department of Oceanography, University of Southampton, Southampton SO9 5NH*

Received 1982 September 1; in original form 1982 June 2

Summary. The tidal dynamics of the South China Sea are examined by the use of a two-dimensional non-linear hydrodynamic finite-difference model which has been run separately for the M_2 and K_1 tidal constituents. The models are tuned through the open boundary conditions to fit the observed coastal tides. Cotidal charts for the two constituents are presented and compared with earlier charts based on coastal observations alone. The flow of tidal energy is studied, and it is concluded that the strength of the diurnal tide in the Sea is due largely to the resonant diurnal response of the Gulfs of Tonkin and Thailand. An energy budget reveals that for both constituents direct tidal forcing within the Sea is significant and that tidal energy which enters through the open boundary is in fact lost back to the Earth–Moon orbital system by this means.

1 Introduction

South of China, bounded by Vietnam to the west, the Philippine Islands to the east and Sarawak in the south, lies the South China Sea (Fig. 1). Stretching 2000 km from north to south, it is over 4 km deep in places and therefore a much more massive body of water than many other semi-enclosed shallow seas, such as its near neighbour the East China Sea. It is connected to the Pacific Ocean by a deep channel to the north-east, the Luzon Strait between Taiwan and the Philippine Island of Luzon. The Taiwan Strait, north of Taiwan, is a much shallower connection to the East China Sea, whilst in the east there are several narrow, shallow connections between the Philippine Islands through the Celebes Sea and eventually to the Pacific Ocean. To the west and south the sea shallows to a broad shelf less than 200 m deep, some 1500 km wide, stretching to Malaysia and up into the Gulf of Thailand, which is taken to be an integral part of the South China Sea. There is a fairly broad, shallow connection with the Java Sea in the south, but from the point of view of studying the tides of the area, it is reasonable to take the southern boundary to lie just north of the equator.

The tides of the South China Sea are of considerable interest for a variety of reasons. Much shipping uses the many ports around the Sea and since the tides can reach several

*On study visit from Shandong College of Oceanography, China.

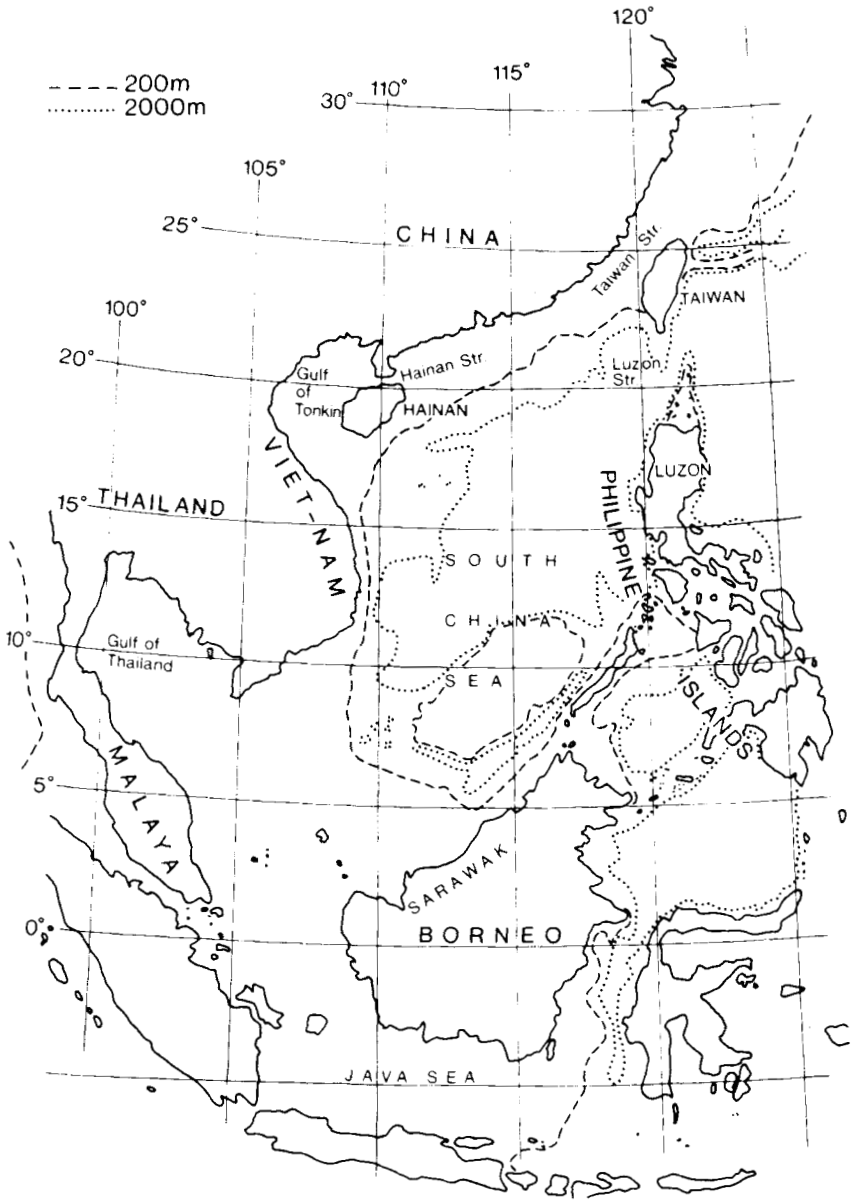

Figure 1. Map of the South China Sea.

metres amplitude they have been relatively well documented over the years. Modern methods of harmonic analysis and prediction are now used for forecasting the tides at the more important ports. A brief survey of the tidal regime at different ports reveals that there is a mixture of semidiurnal, diurnal and mixed tides at different locations. Scientifically, therefore, the Sea is worthy of study in order to discover the dynamical reasons why the diurnal tides are stronger here, relative to the semidiurnal tides, than in most other parts of the world, particularly since the local diurnal astronomical forcing is small at such low latitudes. Commercially, the tidal regime is becoming of increasing importance since a knowledge and understanding of the tidal currents will be important in the development of

offshore platforms used in the search for oil and minerals in the shallower margins of the Sea.

The Sea has therefore attracted some scientific attention, although the tidal regime is by no means well understood. Most of the early work by Dietrich (1944) and others is summarized by Defant (1962) in his section describing 'The tides of the East Indian Archipelago'. He seeks to interpret the cotidal charts drawn by Dietrich from coastal observations in terms of the response of a long channel, forced at either end by the oceanic tides. In the case of the South China Sea, the channel is supposed to have one end at the Luzon Strait driven by the Pacific tides and the other through the Java and Timor Seas driven by the Indian Ocean tides. Defant achieves some measure of success in accounting for the M_2 amphidromic system as a channel with three nodal lines. He further suggests that the channel is close to a resonant length for the diurnal tides, and hence its relatively large amplitude. However, he gives no clear explanation for the significant amplification of the diurnal tides in the Gulf of Tonkin. Moreover, he rightly points out that since the basin has a large area with depths over 4000 m, there may be a significant contribution of tidal energy driven directly by the astronomical forcing, in addition to that forced through the ocean connections which is the basis of his co-oscillating channel theory. Williams (1972) employed an idealized basin oscillator model to show that diurnal amplification in the Gulfs of Tonkin and Thailand is a resonance phenomenon.

Bogdanov & Nefedyev (1961, 1962), have also presented cotidal maps for the M_2 and K_1 constituents which were based on all the coastal and island tidal records then available. Sager (1975) has reviewed the most recently available tidal data for the area and clearly demonstrates the variability of tides around the Sea between diurnal and semidiurnal dominance. His cotidal charts for M_2 and K_1 are revisions of the earlier German charts and provide the most detailed maps to be found. However, all these cotidal maps have essentially been drawn by interpolating between opposite coasts of the Sea, making use where possible of isolated island measurements. No observations of tidal currents appear to be available which would enable a more confident prediction of the offshore tidal state to be made, following the method of Proudman & Doodson (1924), and Robinson (1979) used in European shelf seas. In the deeper parts of the South China Sea, the long wave progression speed will be relatively fast, and the tidal phase might not be expected to vary rapidly with distance, so that interpolation from coastal observations may be acceptable. In the shallower area to the west and into the Gulf of Thailand where this is not the case, coastal records are inadequate for defining the co-tidal patterns offshore.

A more satisfactory method for estimating the offshore tidal conditions is to model the dynamic response of the basin to both direct astronomical forcing and to the tides entering from the adjacent oceans using a numerical model which can be tuned so that predicted coastal tides match the observed values as closely as possible. Such an approach ensures that the predicted tidal regime is dynamically self-consistent, and avoids the pitfalls of over-dependence on tide gauge records. For example the harmonic constants from an old tidal record of dubious quality may be given undue weight in the drafting of a chart if they refer to an island in the middle of a sea, where no other records are available within hundreds of kilometres, whereas a hydrodynamic model may indicate that such a record is anomalous. In addition, some of the coastal records may come from locations inside estuaries, for which there is a significant change of amplitude and phase relative to the adjacent sea area, and these too may mislead the drawing of offshore tidal charts based solely on port observations.

In this paper, therefore, a numerical hydrodynamic model of tidal propagation in the South China Sea is presented, and cotidal charts are drawn from the results. The use of a hydrodynamic model also leads to estimates of energy flux which can indicate both the

dynamical processes controlling the tides, and the extent to which the tides are driven from within by direct astronomical forcing or from outside by the Pacific Ocean. Approximate prediction of offshore tidal currents is also possible from the model.

2 The hydrodynamical model

In order to study the barotropic tide, it is sufficient to use the two-dimensional depth-integrated equations of continuity and momentum for a rotating ocean. Taking into account the effect of the Earth's curvature (since the Sea has a length dimension of the same order of magnitude as the Earth's radius) and the influence of the astronomical tide-generating forces, the non-linear equations are (see, e.g. Davies & Flather 1977 without the wind stress terms).

$$\frac{1}{R\cos\phi}\frac{\partial}{\partial\lambda}(Hu)+\frac{\partial}{\partial\phi}(Hv\cos\phi)+\frac{\partial\zeta}{\partial t}=0 \tag{1}$$

$$\frac{\partial u}{\partial t}+\frac{u}{R\cos\phi}\frac{\partial u}{\partial\lambda}+\frac{v}{R}\frac{\partial u}{\partial\phi}-\frac{uv\tan\phi}{R}-2\Omega v\sin\phi+\frac{ku(u^2+v^2)^{1/2}}{H}+\frac{g}{R\cos\phi}\frac{\partial}{\partial\lambda}(\zeta-\zeta_E)=0 \tag{2}$$

$$\frac{\partial v}{\partial t}+\frac{u}{R\cos\phi}\frac{\partial v}{\partial\lambda}+\frac{v}{R}\frac{\partial v}{\partial\phi}+\frac{u^2\tan\phi}{R}+2\Omega u\sin\phi+\frac{kv(u^2+v^2)^{1/2}}{H}+\frac{g}{R}\frac{\partial}{\partial\phi}(\zeta-\zeta_E)=0 \tag{3}$$

where:

t = time;
λ, ϕ = east longitude and north latitude respectively;
u, v = east and north components of depth mean current;
R = radius of the Earth;
Ω = angular speed of the Earth's rotation;
g = acceleration due to gravity;
k = coefficient of quadratic sea-bed friction, taken as 0.0021 in this case;
H = instantaneous depth from sea surface to sea-bed;
h = local mean depth (or undisturbed depth in the absence of tides);
ζ = $(H-h)$ = elevation of sea surface above the undisturbed level (measured relative to the sea-bed);
ζ_E = sum of the astronomical equilibrium tide and the correction for the effect of the solid Earth tide.

If ζ_0 is the equilibrium tide defined from the astronomical tide-generating potential, then the solid Earth deforms under the influence of the tidal forces so that the sea-bed rises a distance $h_L\zeta_0$. At the same time the redistribution of the Earth's mass effectively increases the tide-generating force by a factor k_L (Hendershott 1972), where h_L and k_L are the tidal effective Love numbers, normally taken to be 0.59 and 0.29 respectively (Munk & MacDonald 1960). Thus the slope of the sea surface relative to an equipotential surface is

$$\partial/\partial x(\zeta+h_L\zeta_0-\zeta_0-k_L\zeta_0)$$

in the x-direction, so that $\zeta_E=\zeta_0(1-h_L+k_L)\simeq 0.7\zeta_0$. No attempt is made to model the effect of the load tide, i.e. the yielding of the Earth under the extra loading of the tidal water movements. Following Cartwright & Taylor (1971), and correcting for the Earth tide, the expressions for the equilibrium tide for the M_2 and K_1 constituents to be investigated are:

$$\zeta_E(M_2)=0.168\cos^2\phi\cos[\sigma(M_2)\,t+2\lambda]\ \text{m} \tag{4}$$

and

$$\zeta_E(K_1) = 0.098 \sin 2\phi \cos[\sigma(K_1)\, t + \lambda + \pi] \text{ m}. \quad (5)$$

Equations (1–3) were solved numerically in finite difference form following a scheme similar to that used by Flather & Davies (1975). This is an explicit technique which generates solutions through space and time. The grid which is used defines the elevation at the centre of grid squares, the northward velocity at the centre of the north and south boundaries of each box and the eastward velocity at the east and west boundaries. Along the coastal boundaries of the model the velocity normal to the boundary is required to be zero. At open boundaries a condition on the elevation, or relating the elevation to the velocity, must be imposed.

Care must be taken with finite difference modelling of the non-linear terms in the equation, but in this case it was found that the non-linear advective terms were very small. Indeed, their neglect along with the curvature terms in a development phase of the model led to results very similar to those achieved with the full equations.

The South China Sea was divided into the network of curvilinear grid squares shown in Fig. 2, each grid being 0.3125° in latitude and 0.3125° in longitude. Although such a fine grid is probably unnecessary for representing the tidal patterns in the deep area, it is demanded in order to resolve in sufficient detail the amphidromic systems in the shallower margins. Given the computing power now available on modern computers it was not worth considering a mixed grid such as that used by Greenberg (1975). The approximate value of h in each of the 2712 grid squares was obtained from the UK Admiralty Chart No. 1263 and a weak smoothing process was applied to the depth array before its use in the tidal computations. In the grid scheme chosen, there are five open boundaries (see Fig. 2), two major

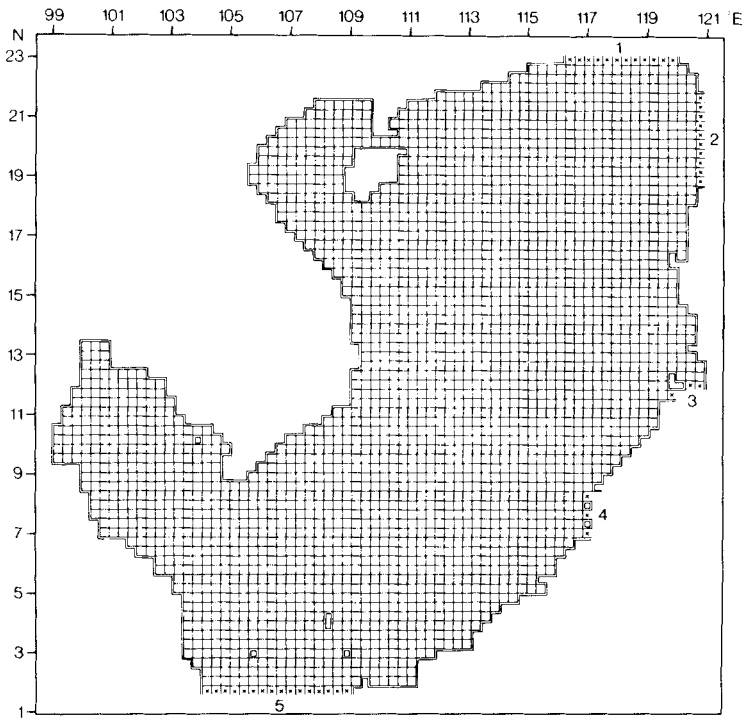

Figure 2. Finite difference grid used to model the South China Sea. Solid boundaries, ═══. Open boundaries, X X X X.

ones in the north-east, and one in the south, with two small openings in the east representing the very shallow channels between the Philippine Islands. Simple boundary conditions of imposed elevation were applied at the open boundaries, the elevation phase and amplitude being estimated from local tidal observations. Interpolation across the wider boundaries was performed with the help of the cotidal charts of Sager (1975), although the opportunity was taken to adjust the boundary elevations slightly in order to tune the model to match the observed coastal data as well as possible throughout the Sea.

A time step of 98.6 s was used in the finite difference solution, which is within the Courant stability criterion. Starting with an initially flat surface, the model was run out for nine tidal cycles, by which time a sufficiently steady tidal repeat cycle had been achieved. The M_2 and K_1 constituents were computed in separate runs, and the tidal amplitude and phase in each grid square was obtained by Fourier analysis of the elevations over the final cycle. Although it would be highly desirable to run M_2 and K_1 together in order to model their interaction through quadratic friction, to do so would have required much longer runs in order to separate the longer period modulations which occur because the M_2 frequency is not a simple multiple of K_1. This would also lead to difficulties in confirming that the solutions had converged to a steady repeat cycle. Furthermore, it would be harder to tune the model to fit both the M_2 and the K_1 observations. It was therefore concluded that it

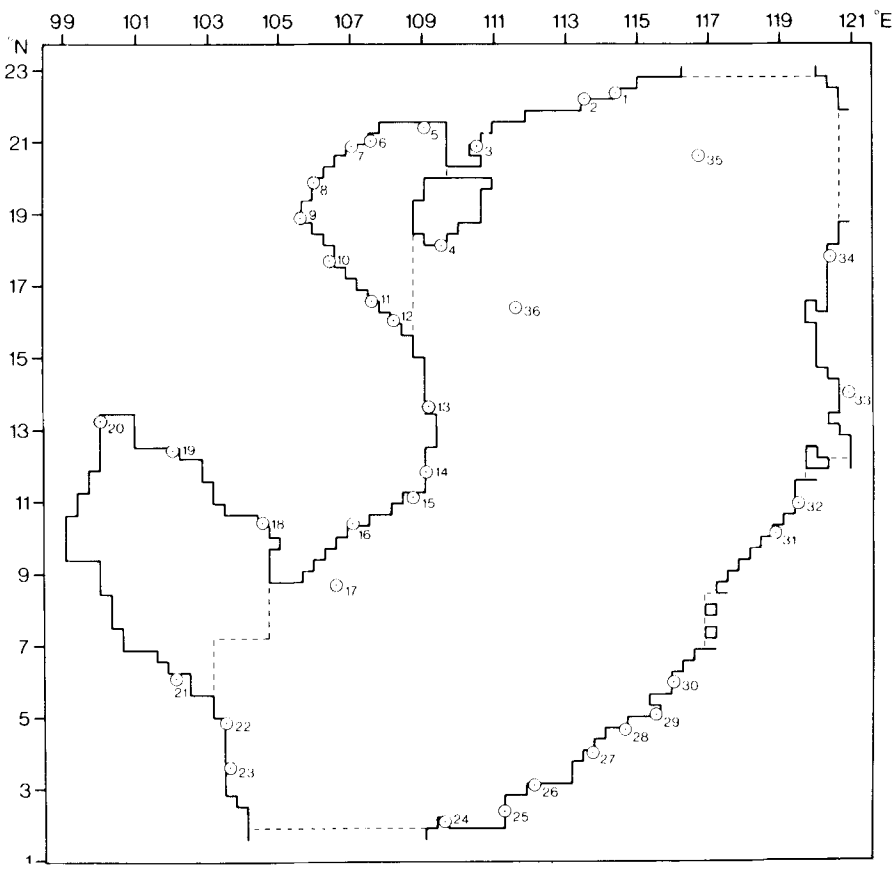

Figure 3. Locations of coastal tidal data stations relative to the model grid and boundaries used for the energy budget (– – –).

M_2

	Station		Observation		Computation		Observation		Computation	
	Latitude	Longitude	Amplitude (cm)	Phase (°)	Amplitude (cm)	Phase (°)	Amplitude (cm)	Phase (°)	Amplitude (cm)	Phase (°)
1	22°28′	114°20′	39	253	36	249	36	296	33	279
2	22°12′	113°33′	47	283	44	256	37	300	36	282
3	20°57′	110°36′	79	304	86	302	41	310	45	306
4	18°13′	109°32′	20	303	19	305	29	310	33	308
5	21°29′	109°06′	38	179	49	178	103	76	100	77
6	21°02′	107°22′	19	162	20	170	72	83	89	82
7	20°53′	107°04′	7	126	3	120	41	310	80	85
8	19°55′	106°01′	18	0	30	30	68	92	65	89
9	18°48′	105°46′	30	11	37	34	50	88	61	95
10	17°42′	106°28′	18	23	17	13	22	97	26	95
11	16°34′	107°37′	18	334	16	332	3	258	3	258
12	16°07′	108°18′	16	302	18	312	19	277	21	284
13	13°45′	109°13′	19	303	17	314	32	286	35	294
14	11°53′	109°12′	20	316	17	325	35	296	37	295
15	11°10′	108°42′	22	331	23	342	40	292	40	295
16	10°24′	107°01′	80	54	92	65	70	309	62	305
17	08°41′	106°36′	80	62	87	65	64	319	63	317
18	10°22′	104°28′	10	96	28	84	27	65	26	70
19	12°28′	102°04′	17	96	35	96	59	159	57	139
20	13°21′	100°00′	46	140	41	236	66	168	100	167
21	06°12′	102°10′	19	248	42	264	30	331	32	331
22	04°47′	103°26′	38	225	54	230	57	349	58	341
23	03°32′	103°28′	60	240	70	234	51	3	55	351
24	02°05′	109°39′	90	105	80	90	35	325	44	319
25	02°09′	111°15′	142	112	120	75	48	336	54	313
26	02°54′	112°05′	36	93	65	67	40	326	50	307
27	03°58′	113°42′	17	343	24	357	40	316	41	302
28	04°37′	114°39′	21	323	20	346	31	313	28	301
29	05°05′	115°33′	28	325	23	338	40	316	40	301
30	05°19′	116°04′	24	319	20	335	37	311	39	301
31	10°04′	118°46′	20	310	16	305	33	316	31	300
32	10°53′	119°25′	23	316	16	299	33	323	32	299
33	13°46′	120°55′	24	311	15	287	29	314	30	298
34	17°47′	120°25′	8	237	11	239	19	317	21	299
35	20°41′	116°43′	14	257	17	245	27	314	26	282
36	16°33′	111°37′	17	292	16	296	27	297	32	294

would be more satisfactory in the first instance to study the components individually in order to determine the broad features of the dynamic response. To some extent the interaction effects are compensated for by seeking to match the model to the observations.

The only observational data available against which to test the validity of the model results are the harmonic constants for M_2 and K_1 from ports around the Sea, at the locations marked on Fig. 3. These were obtained from the archives of the Bidston Laboratory of IOS and are essentially those to be found in the IHB lists. As discussed by Sager (1975) they are of variable quality, some being several decades old, and some obtained from data spans as short as 15 days which must inevitably be corrupted by both long-period constituents and modulation by unresolved constituents at nearby frequencies. Further differences in comparison between model predictions and observations are to be expected since the model grid cannot represent the fine detail of coastline topography and it is not always possible to match a port's true location accurately with its appropriate grid square on the model. Moreover, the model can in no way represent any very local dynamical processes in estuaries and coastal embayments which result in port tides not being representative of the tides in the immediate offshore area.

Despite these problems, the agreement between the modelled and observed coastal tides is encouragingly close, as indicated by Table 1, both for amplitude and phase. For comparison purposes, the phases have all been reduced relative to time zone 8, i.e. to eight hours before the Moon's transit at Greenwich. The K_1 results are particularly close to the observations, the phases agreeing to within better than 5° in most cases and nowhere worse than 20°, and the amplitudes mostly less than 10 per cent different. The M_2 agreement is not quite so good, but this may reflect the problem of local variability mentioned above which is a greater problem for higher tidal frequencies.

Since it was possible to achieve this reasonable match between model and observations over the whole Sea by small adjustments to the imposed boundary conditions on elevation, no attempt was made to tune the model further by variations in the bottom friction coefficient. To vary k would alter the overall energy dissipation and influence the energy budget. However, in the absence of reliable tidal stream observations with which to compare the model predicted velocities and hence energy fluxes, any variation of k from the value which has been used satisfactorily in models of other shelf seas would have been completely arbitrary and was therefore not attempted. This, and the independent running of the M_2 and K_1 constituents, qualify the conclusions drawn in Section 4 on the energy, but should have little effect on the results presented in the next section.

3 Cotidal charts

Since the model is able to predict the coastal observations with some success, albeit through tuning the model by choosing appropriate open-boundary elevations, then the offshore elevations predicted by the model may be taken to be sensible estimates of the true tidal conditions, since they are dynamically self-consistent in so far as equations (1–3) are representative of the real Sea dynamics. Given the offshore amplitude and phase in each grid square, it was a simple exercise to draw the cotidal charts for M_2 and K_1 which are displayed in Figs 4 and 5 respectively.

The overall pattern is similar in broad outline to the earlier charts of Dietrich and Sager, since the coastal observations on which they are based are the same, but there are some significant differences in detail. In comparison with Sager's charts, it should be noted that his phases are based on a time zone seven hours ahead of Greenwich. The M_2 tide clearly progresses from the Pacific Ocean through the Luzon Strait (open boundary 2) and south-

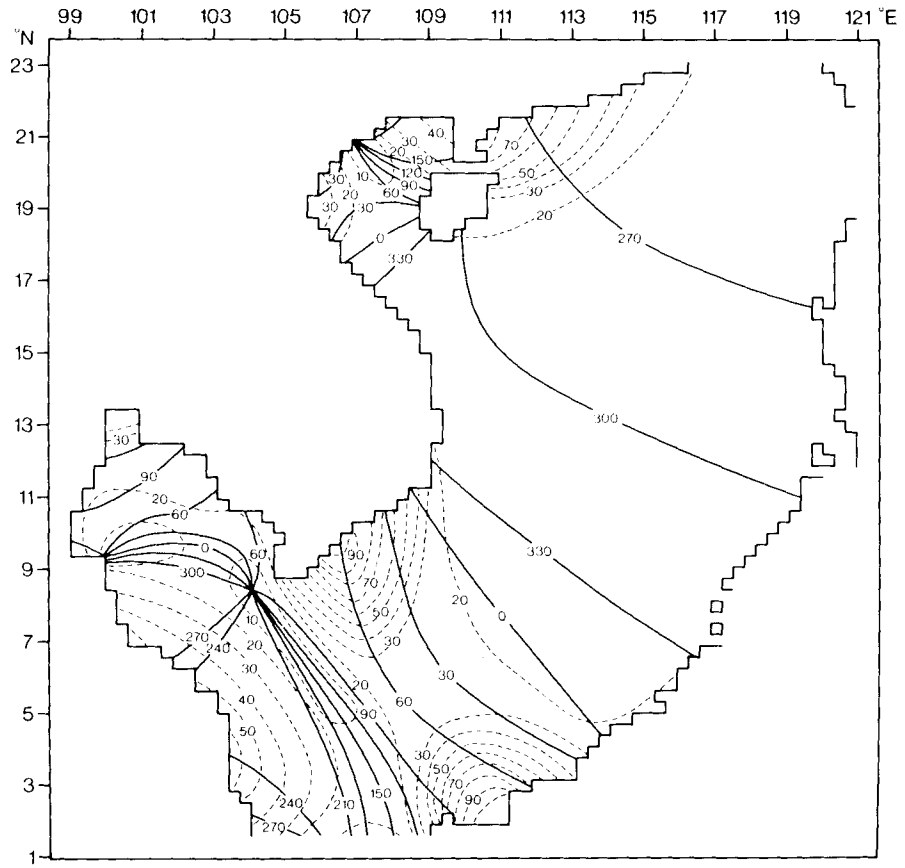

Figure 4. M_2 cotidal chart: —— phase in degrees relative to 8 hr before Greenwich, – – – amplitude, cm.

westwards through the main part of the Sea. The wide spacing of the cotidal lines is indicative of the high speed of the tidal wave (approximately 600 km hr^{-1}) which is appropriate to such deep water, rather than of a standing wave which appears to be indicated in Dietrich's chart. Over the deep basin, the model tides are nearly double the height of those suggested by Sager. The steep increase in amplitude from 20 cm over most of the northern basin to more than 70 cm along the south-east China coast may be due partly to the Corolis effect resulting in a Kelvin wave propagating along the Chinese coast. The M_2 tidal response of the Gulf of Tonkin is quite complex. The tide progresses northwards into the Gulf, but whilst the amplitude increases to the west and north-east corners, along the northern coast it is reduced almost to zero. The amplitude here is in good agreement with Sager, but both he and Dietrich suggest the presence of an amphidrome which in the model phase results has become degenerate. It is worth pointing out here that whilst the position or even the existence of an amphidromic point appears to be an important feature of a cotidal chart, and the eye is clearly attracted to amphidromes in the comparison of different charts, in terms of practical importance the exact position of the amphidrome is not so significant. What is important is that a region of low amplitudes is predicted in the correct location, and within that region because the tidal constituent will be small compared with other constituents its phase is not important. The M_2 tide appears to oscillate in the Tonkin Gulf with approximately half a wavelength between the Vietnamese coast to the west and the north-eastern

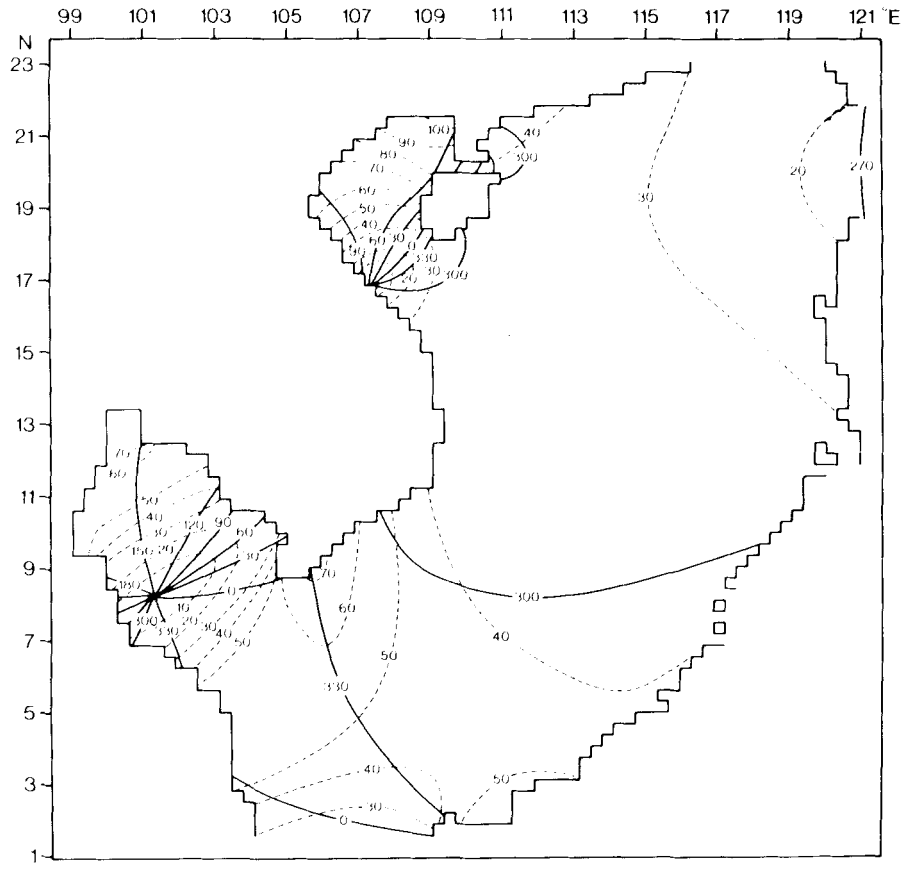

Figure 5. K_1 cotidal chart: —— phase in degrees relative to 8 hr before Greenwich, – – – amplitude, cm.

end of the Gulf. There is almost a nodel line between Haiphong and the Island of Hainan, and this results in the almost purely diurnal tides which are found in this area.

The M_2 model results do predict an amphidrome in the Gulf of Thailand, but close inspection shows that this is unusually a clockwise rotating system. The amphidrome of Sager appears to have become a degenerate amphidrome in the west Thailand coast. A clockwise amphidrome is found in the chart of Bogdanov & Nefedyev (1961). Once again, there is no great significance to the details of the phase patterns when both Sager's chart and the model results agree that there is effectively a nodal line of very low amplitude running north-west to south-east out of the Gulf of Thailand into the main South China Sea. To the west, and to the north of the Gulf of Thailand the amplitude increases and the impression is given of another half-wave oscillation between Bangkok in the north and the Malayan peninsula in the south. The strong amplitude amplification which is predicted by Sager's results to occur off southern Vietnam and off the north-west corner of Borneo is also found in the model results. This cannot be a standing oscillation from north to south across the sea, since the phases are the same at each coast. On the other hand it may well be the result of two standing oscillations, one between the Malayan coast and the south of Vietnam, separated by the nodal region of low amplitude, and the other between Malaya and the north coast of Borneo. The phases match such a hypothesis, and it is not unreasonable to postulate standing oscillations across the open sea at low latitudes where the Coriolis effect is too weak to force the phase pattern into an amphidromic system. There is apparently also

amplification of the tide due to the shallowing depth hear the coast. Thus overall, it appears that the general south-westward propagation of the tide is distorted by at least three localized standing oscillations.

The broad pattern of K_1 propagation is similar to M_2, with a rapid movement of the tide from north-east towards the south-west. This is accompanied by a steady increase of amplitude from 20 cm in the Luzon Strait to 40–50 cm between Vietnam and Borneo. The amplification is not limited to the coastal margin as suggested by Sager, and dynamically it implies that the whole Sea may have a natural period quite close to the diurnal periodicity. As for M_2, there are localized phase patterns within the Gulfs of Tonkin and Thailand. The former appears to be slightly longer than a quarter-wavelength for K_1, resulting in a nodal region near the mouth which is shifted by the friction effect to the left of the inwardly propagating wave. In the model the resulting amphidrome is just on the coast, whilst Sager's chart shows it further offshore. The predicted amplitudes are close to those observed, reaching 100 cm at the head and enhancing the diurnal dominance in this area. For both M_2 and K_1, the connection through the Hainan Strait appears to have little dynamical significance.

The amplitude increases in the coastal area around Saigon, but to a lesser extent in the model than in Sager's chart where the mid-sea amplitudes are lower. It is not so easy to attribute this to a cross-sea oscillation as for M_2, since there is little amplification along the north-west Borneo coast. It may therefore be largely a topographic amplification as the tide propagates into shallower water. The Gulf of Thailand is also slightly longer than a quarter-wavelength. The nodal area near the mouth and the amphidrome predicted by the model agree closely with Sager's chart.

Overall, although the amplitude of M_2 and K_1 are both about 20 cm at the north-east connection with the Pacific, the Sea appears to respond more strongly to the diurnal, leading to a mixed tide, diurnally dominant along most of the coastline. This is distorted locally by amphidromes, and local gulf oscillations, leading to pure diurnal tides in some places and more unexpectedly to strongly semidiurnal tides in others.

4 Tidal energy

Whilst cotidal maps give a good indication of the tidal wave propagation through a region, and show where gulfs are co-oscillating, they do not make clear the progression of dynamical cause and effect, i.e. which area of sea contains the forcing tides, and which area is responding to that forcing. For this purpose, the energy fluxes which can readily be predicted from the model results are more illuminating.

If the constituent elevation amplitude is Z and its phase ϕ_z, and the east velocity has amplitude U and phase ϕ_u, then the apparent mean energy flow over a cycle of the tidal harmonic is $\frac{1}{2}\rho g\, ZUh \cos(\phi_z - \phi_u)$ through unit width of a vertical plane lying along a meridian. Similarly the northward flow across a parallel of latitude is $\frac{1}{2}\rho g\, ZVh \cos(\phi_z - \phi_v)$ per unit width. Hence the energy flow per unit width through each side of a grid square can be estimated from the prediction of east and north velocity, and using for the elevation along the sides of grid squares the average of elevation predictions for the two adjacent grid square centres. The vector average of the energy flow through each of the sides gives an indication of the direction and magnitude of the total mean energy flow associated with that tidal harmonic, per unit width normal to the flow direction. These vectors are shown plotted for M_2 and K_1 in Figs 6 and 7.

In Fig. 6, the mean energy carried by the M_2 wave is seen to enter entirely through open boundary 2, i.e. the Luzon Strait. There is virtually no energy transport through boundary 1, the Taiwan Strait, or 3 and 4, the gaps between the Philippines. Nearly all the energy flows

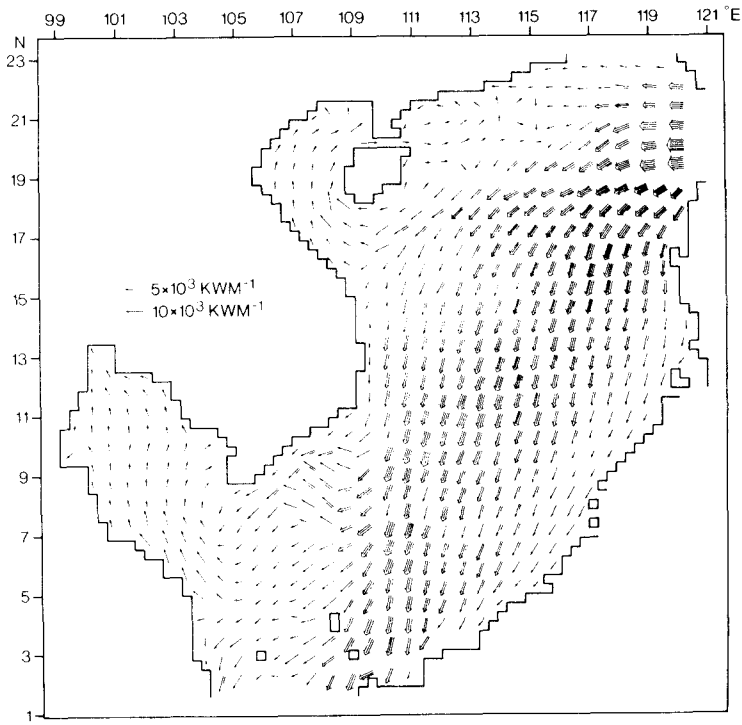

Figure 6. M_2 energy flux vectors. The key shows the magnitude of power per unit width normal to the vectors.

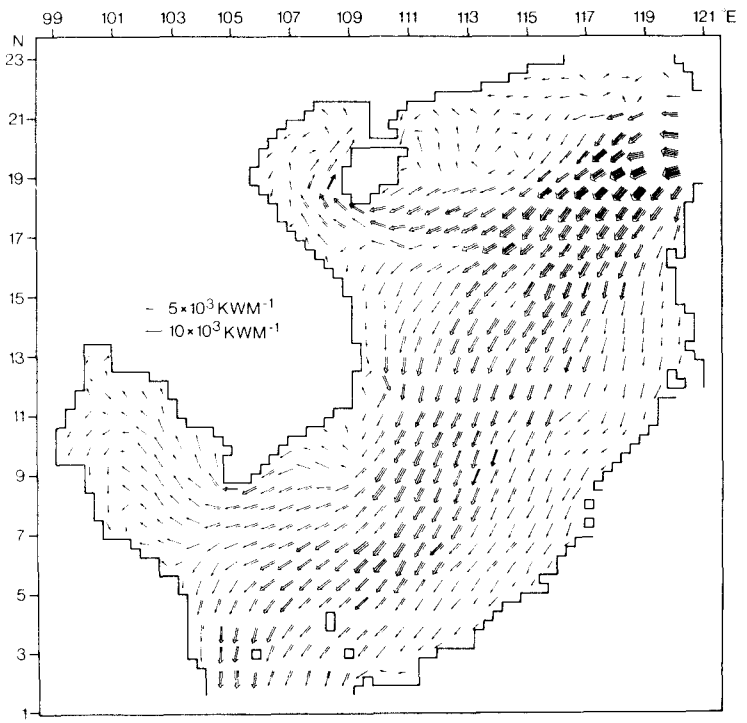

Figure 7. K_1 energy flux vectors. The key shows the magnitude of power per unit width normal to the vectors.

southwards through the main basin, losing some energy towards the coastlines and with a significant flow into the Gulf of Tonkin. Some energy flows right through the Sea and out through the southern open boundary 5. There is a noticeable reduction in the energy flux west of 110°E, suggesting that significant energy dissipation occurs between southern Vietnam and western Borneo, which is where the Sea becomes much shallower and also where a strong amplification of the M_2 tide was observed in the cotidal charts. Some of the energy flows on into the Gulf of Thailand, and in its entrance there is a clockwise energy gyre, which corresponds to the clockwise rotating amphidromic system.

Whilst the K_1 energy flows in Fig. 7 are broadly similar to M_2 it is noticeable that much more of the energy entering from the Pacific appears to be diverted into the Gulf of Tonkin, indicating that it is close to resonance. There is also a less marked decrease in flux west of 110°E since there is little amplification of the tide along the NW Borneo coast, although the area around Saigon remains an energy sink. Energy flows directly into the Gulf of Thailand, without the gyre noted in M_2. Overall, a comparison between the two constituents suggests that the major differences in tidal response between the diurnal and semidiurnal tides are a result of the different dynamic responses of the Gulfs, rather than of the Sea as a whole.

Figs 6 and 7 do not indicate whether significant energy is being input by the astronomical forcing. To explore this it is necessary to establish an overall energy budget for the area, similar to that performed by Robinson (1979) for the Irish Sea, only using model predicted tides rather than those observed offshore. The mean energy balance equation given by Garrett (1975) for a region G bounded by a boundary M is:

$$-\int_M \rho g h\, \overline{\mathbf{v}\zeta}\cdot\mathbf{n}\,ds + \int_M \rho g h\, \overline{\mathbf{v}\zeta_E}\cdot\mathbf{n}\,ds + \int_G \rho g\, \zeta_E \frac{\partial \zeta}{\partial t}\,dA = \int_G \mathbf{F}\cdot\mathbf{v}\,dA. \tag{6}$$

$\mathbf{n}$ is an outward unit normal to the element ds of the boundary and dA is an element of the surface area. $\mathbf{F}$ is the friction force associated with the tidal flow. If the dynamics can be considered to be essentially linear, then equation (6) can be applied to individual tidal constituents. Now the non-linear advective and curvature terms were found to have very little influence in the running of this particular model, so that non-linear interactions between constituents due to those terms can be neglected. However, there is bound to be significant interaction between constituents through the quadratic bottom friction, particularly in a case such as the South China Sea where the M_2 and K_1 amplitudes are similar. This is something it was not possible to model since the constituents were run independently, and to this extent the calculation of the energy budget will lack an essential, though hopefully small input to the energy balance which is present in the actual Sea. With this qualification, the terms of equation (6) can be interpreted as follows for an individual tidal harmonic.

The first term T_1 is the apparent energy flux associated with the tidal wave crossing the boundary, and is the same as the energy flux already plotted throughout the region in Figs 6 and 7. It is the energy flow that would occur if the tidal rise and fall occurred in the absence of any tide generating forces or Earth tide movement. The second term T_2 is an adjustment to the energy budget to allow for both the work done by the tide-generating force across the boundaries, and also the correction for Earth tide movement at the boundaries. The third term T_3 is the work done on the Sea throughout the area by the effect of the sea surface moving through a potential field which is itself varying with time. Like T_2 this includes a contribution from the tide-generating forces and a negative contribution (−30 per cent of the TGF) from the Earth tide movement. If desired the total work done by the tide-generating force on the Sea within the region G could therefore be calculated as $10/7(T_2 + T_3)$, and the work done by the Sea on the solid Earth would be $3/7(T_2 + T_3)$. However, in our calculations we have not distinguished between the Earth tide and astro-

nomical forcing aspects of T_2 and T_3 since we are particularly interested in the relative magnitudes of T_1 and $(T_2 + T_3)$, i.e. the extent to which the tides in the Sea are driven from the outside ocean in comparison to internal forcing.

T_1 and T_2 have been evaluated from the harmonic constituents of elevation and velocity (following Robinson 1979) at the five open boundaries of the model, and also at two internal boundaries across the mouth of the Gulfs of Tonkin and Thailand (see Fig. 3). T_3 has been evaluated over the whole area, and over the subareas of the two Gulfs. The resulting energy balances are listed in Table 2 for both constituents. The dissipation term on the rhs of equation (6) has not been calculated directly by estimating **F** from the model, since this would involve a numerical integration in time rather than simply using the harmonic constituents as for T_1, T_2 and T_3. Rather it is assumed that with an energy conserving finite difference scheme the balance is satisfied by the model anyway, and the sum of T_1, T_2 and T_3 yields the net energy dissipation.

The model results over the whole area are most interesting. Garrett (1975) suggests that whilst T_2 and T_3 may be relatively large compared with T_1, they will generally be of opposite sign and their sum quite small. This is indeed true of the shallow Gulfs and Garrett was considering such shallow enclosed embayments in his discussion. For the whole of the Sea, however, the astronomical forcing/Earth tide energy contribution is the same order as that entering from the external tide – in the case of M_2 it is nearly half, and for K_1 nearly a quarter. In both cases it is in fact negative, which means that some of the energy entering through the boundary is being lost doing work against the astronomical forcing. Given the reasonable agreement between the observed and modelled elevation phases, this is a result which should not be strongly dependent on the accurate modelling of the energy dissipation. There are interesting implications for global tidal energy budgets such as that performed by Miller (1966). He estimated the M_2 energy flux entering through the Luzon Strait to be 5.0 GW. This is considerably less than predicted by the model. However, even if an accurate measurement could be made of energy entering a large enclosed basin such as the South China Sea, by means of current meters and tide gauges, it would be wrong to assume, as Miller does, that this is all energy lost from the Earth–Moon orbital system, since in fact the model suggests that half of it (in the case of M_2) is fed back into orbital energy from within the basin.

Table 2. Mean rate of tidal energy flow (GW).

	K_1			M_2		
	Entire Sea	Gulf of Tonkin	Gulf of Thailand	Entire Sea	Gulf of Tonkin	Gulf of Thailand
T_1, apparent influx across boundaries	16.06	3.56	3.30	25.78	0.902	1.94
T_2, work done by astronomical forcing and Earth tides across boundaries	−12.78	1.37	0.29	12.16	−0.212	1.51
T_3, work done by astronomical forcing and Earth tides on enclosed water mass	9.30	−1.23	−0.57	−24.46	0.188	−1.69
$T_2 + T_3$, total work done by Earth tides and astronomical forcing	−3.48	0.14	−0.28	−12.30	−0.024	−0.18
$T_2 + T_3 + T_1$, mean rate of frictional dissipation	12.58	3.70	3.02	13.48	0.878	1.76

The M_2 and K_1 total energy dissipation are similar in magnitude, but distributed very differently. Over half of the diurnal energy dissipated in the whole Sea is accounted for in the two Gulfs, whilst for M_2 the fraction is only about one-fifth. In both Gulfs the actual diurnal dissipation is much greater than the semidiurnal, and the Gulfs appear to be acting as tuned oscillators drawing in diurnal energy from the Pacific tides.

5 Tidal stream amplitudes

In Figs 8 and 9 are plotted the approximate distribution of maximum tidal streams, for the model runs of M_2 and K_1 respectively. These must be treated with some caution since whilst the prediction of elevation with a model can usually be quite successful, currents vary locally because of small-scale topographic features. In the Hainan Strait, for example, tidal streams will be large, but are not adequately resolved on this model grid. The figures are therefore only a general indication of where the tidal streams are weak or negligible and where they are likely to be important for offshore civil engineering activities.

The distributions of current reflect what has already been observed about the elevations. Thus K_1 streams are seen to be largest in the Gulfs of Tonkin and Thailand, whereas the M_2 streams find their maximum off the south coast of Vietnam and to the north and west of Borneo. Maximum K_1 currents are over $50\,\mathrm{cm\,s^{-1}}$ in the Gulf of Tonkin, whilst the M_2 maximum is only $35\,\mathrm{cm\,s^{-1}}$ off the Borneo coast near the southern open boundary. Indeed, overall the K_1 streams tend to be greater than M_2, and this is noticeable over the deepest part of the Sea, although for practical purposes the streams here are negligible. However, in the shallow area bounded by Malaya, Vietnam and Borneo, the M_2 streams are in general

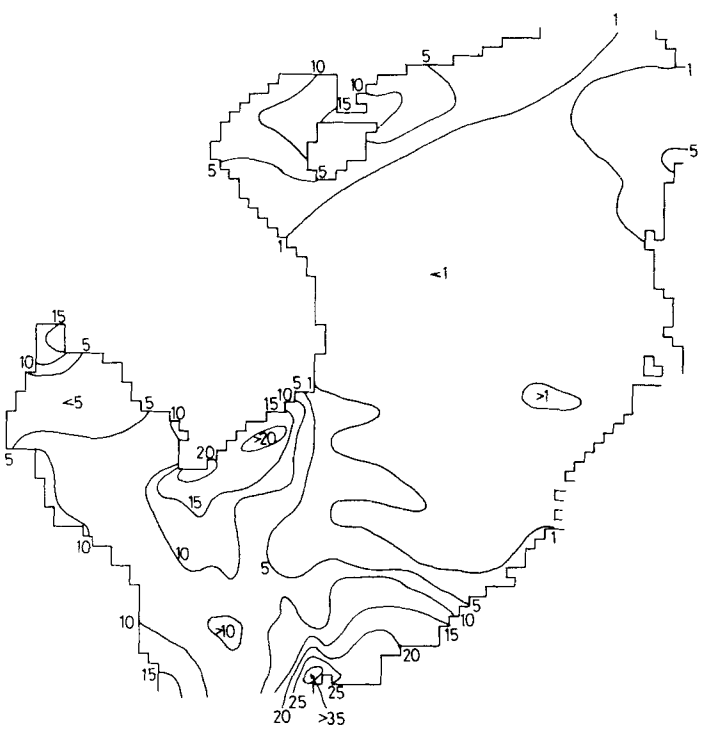

Figure 8. M_2 tidal stream amplitudes. Contours in $\mathrm{cm\,s^{-1}}$.

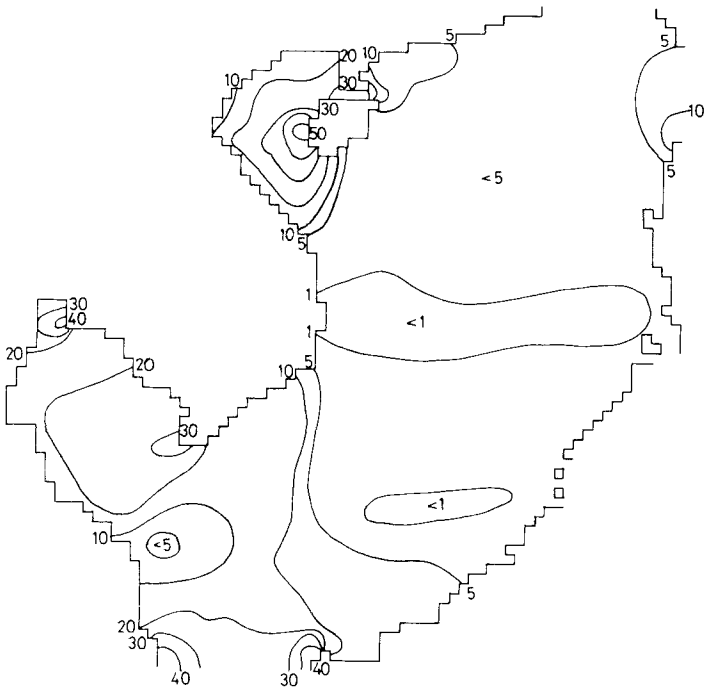

Figure 9. K_1 tidal stream amplitudes. Contours in cm s^{-1}.

strongest, and this must contribute significantly to the M_2 energy dissipation, enabling it to be slightly greater than the overall K_1 dissipation.

It should be remembered that practical forecasting of maximum currents should incorporate all the important tidal constituents, but it may reasonably be assumed that M_2 and K_1 reflect the typical semidiurnal and diurnal distribution respectively. Thus whilst the maximum sum of K_1 and M_2 is around 60–70 cm s^{-1}, the actual stream maxima are likely to be in excess of 1 m s^{-1} when all the constituents are in phase.

6 Conclusions

The model appears to be capable of reproducing the M_2 and K_1 tidal constituents observed at coastal stations around the South China Sea, with realistic boundary conditions on the elevation. The resulting offshore predictions of elevation are therefore considered to be a sound basis for the production of cotidal charts of the area, although ideally they require the confirmation of either offshore tide gauge records, or at least deductions from tidal stream measurements. The model can also be used to indicate tidal stream amplitudes. These are very small over most of the Sea, but some regions where tidal streams may be significant to offshore exploration operations have been identified.

The energy budget based on the model confirms the suggestion that to some extent the whole Sea, but particularly the Gulfs of Tonkin and Thailand, are dynamically much more responsive to diurnal than semidiurnal forcing, and this accounts for such strong diurnal tidal elevations in an area so close to the equator. Further clarification of how close the basin is to a diurnal resonance might be obtained by examining the basin response to a vareity of different mouth forcing frequencies. The conclusion from the energy budget is that there is no resonance with the direct tidal forcing which on the contrary acts to hinder

the tidal oscillation. Finally it should be recalled that the division of semidiurnal and diurnal tides into separate model runs is not strictly justified in a region of mixed tides. It would be an important further exercise to run the M_2 and K_1 tides together and explore their interaction – in particular the influence of each on the dissipation of the other.

Acknowledgment

The assistance of Mr David Blackman of IOS (Bidston) in supplying the harmonic constituents for the South China Sea is gratefully acknowledged.

References

Bogdanov, K. T. & Nefedyev, V. P., 1961. New daily charts of the many-day tidal waves (M_2 and S_2) in the waters between Austrlia and Asia, *Dokl. Akad. Nauk. SSSR*, **141**, 1078–1081 (pp. 1255–1257 in English translation).

Bogdanov, K. T. & Nefedyev, V. P., 1962. New cotidal charts of diurnal tidal waves (K_1 and O_1) in Asiatic and Australian Seas, *Dokl. Akad. Nauk. SSSR*, **144**, 1034–1037 (pp. 14–16 in English translation).

Cartwright, D. E. & Taylor, J., 1971. New computations of the tide-generating potential, *Geophys. J. R. astr. Soc.*, **23**, 45–74.

Davies, A. M. & Flather, R. A., 1977. Computation of storm surge of 1–6 April 1973 using numerical models of the N.W. European Continental Shelf and the North Sea, *Dt. Hydrogr. Z.*, **30**, 139–162.

Defant, A., 1961. *Physical Oceanography*, vol. II. Pergamon Press, Oxford.

Dietrich, G., 1944. Die Gezeiten des Weltmeeres als geograph, *Erseheinung Z. d. ges. Erdkunde*, p. 69, Berlin.

Flather, R. A. & Davies, A. M., 1975. The application of numerical models to storm surge prediction, *Rep. Inst. Oceanogr. Sci., U.K. No. 16*, 23 pp.

Garrett, C., 1975. Tides in gulfs, *Deep Sea Res.*, **22**, 23–35.

Greenberg, D. A., 1975. Mathematical studies of tidal behaviour in the Bay of Fundy, *PhD thesis*, University of Liverpool, 139 pp.

Hendershott, M. C., 1972. The effects of solid earth deformation on global ocean tides, *Geophys. J. R. astr. Soc.*, **29**, 389–402.

International Hydrographic Bureau – Tides. List of harmonic constants, *Spec. Publs int. hydrogr. Bur. No. 26*.

Miller, G. R., 1966. The flux of tidal energy out of the deep oceans, *J. geophys. Res.*, **71**, 2485–2489.

Munk, W. & MacDonald, G. J. F., 1960. *The Rotation of the Earth*, Cambridge University Press.

Proudman, J. & Doodson, A. T., 1924. The principal constituent of the tides of the North Sea, *Phil. Trans. R. Soc. A*, **224**, 185–219.

Robinson, I. S., 1979. The tidal dynamics of the Irish and Celtic Seas, *Geophys. J. R. astr. Soc.*, **56**, 159–197.

Sager, G., 1975. Die Gezeiten des Südchinesischen Meeres, *Beitr. Meereskunde*, **36**, 95–110.

Williams, N. V., 1972. The application of resonators and other methods to problems in oceanography, *PhD dissertation*, University of New South Wales, Australia.